PUBLICAÇÕES

IFUSP/P-829

BACK-ANGLE ANOMALY AND COUPLING BETWEEN SEVEN REACTION CHANNELS OF $^{12}C+^{24}Mg$ USING ALGEBRAIC SCATTERING THEORY

A. Lépine-Szily, M.M. Obuti, R. Lichtenthäler Filho,
J.M. Oliveira Jr. and A.C.C. Villari
Instituto de Física, Universidade de São Paulo

Março/1990

BACK-ANGLE ANOMALY AND COUPLING BETWEEN SEVEN REACTION CHANNELS OF $^{12}C + ^{24}Mg$ USING ALGEBRAIC SCATTERING THEORY

A. Lépine-Szily, M.M. Obuti, R. Lichtenthäler Filho, J.M. Oliveira Jr. and A.C.C. Villari

Deptº de Física Nuclear - Instituto de Física da Universidade de São Paulo - Caixa Postal 20516 - 01498 São Paulo, SP - Brasil

ABSTRACT

We measured six fairly complete angular distributions of elastic, inelastic and α-transfer reactions of the $^{12}C+^{24}Mg$ system at E_{CM} = 25.2 MeV. We performed coupled channels calculations using the Algebraic Scattering Theory with nuclear algebraic potential derived from nuclear phase shifts and using available structure informations for the inelastic coupling strengths. The back angle rise in the elastic cross section is fully explained by the couplings between elastic and transfer channels.

Angular distributions of elastic and inelastic scattering and α-transfer reactions between nα type nuclei of the s-d shell present oscillating shapes with strong rise in the backward angular region[1,2]. Recent studies[3,4] of the $^{24}Mg+^{16}O$ system have indicated that the coupling between elastic and ground state α-transfer channels can have an important contribution to explain the back angle anomalies observed in the elastic, inelastic and transfer cross-sections. The recent work of Alhassid and Iachello[5,6] has shown that their Algebraic Scattering Theory (AST) can be applied to heavy ion reactions, allowing the coupling of several reaction channels.

We applied the AST to our seven reaction channel data on $^{12}C+^{24}Mg$ system to show the correlation between channel couplings and backward anomalies. We also derived the ℓ-dependence of the nuclear algebraic potential from nuclear phase shifts and used it in our seven coupled-channels AST calculations. Details of the AST should be found in references 5 and 6 and references therein.

In the algebraic approach the functional form of the S-matrix is determined from assumptions about the dynamic symmetry of the relative motion of colliding particles. No explicit reference is made to potentials and Schrödinger equation; the cross sections are directly calculated from the S-matrix. The main advantage of this algebraic approach is that the multichannel situation can be easily generalized from the one-channel problem, solving a set of coupled algebraic equations instead of coupled differential equations.

In the case of heavy ion scattering near the Coulomb barrier, Alhassid and Iachello[5,6] assumed that the S-matrix derived from SO(3,1) algebra (eq. 1) is valid in the presence of the nuclear potential:

$$S_\ell(k) = \frac{\Gamma(\ell+1+iv(\ell,k))}{\Gamma(\ell+1-iv(\ell,k))} \qquad (1)$$

where the total algebraic potential $v(\ell,k)$ can be written as:

$$v(\ell,k) = v_c(k) + v_N(\ell,k) = \frac{\mu Z_1 Z_2 e^2}{\hbar^2 k} + v_N(\ell,k) \qquad (2)$$

where $v_N(\ell,k)$ is called the algebraic nuclear potential and absorption can be taken into account by making $v_N(\ell,k)$ complex. Data can be analyzed using simple models for the ℓ-dependence of $v_N(\ell,k)$. and Alhassid-Iachello used a Woods-Saxon ℓ-dependence to analyse the data of $^{18}O+^{24}Mg$ at 27.8 MeV[5,6].

However, it seemed interesting to deteraine the ℓ-dependence of the algebraic nuclear potential that corresponds to a Woods-Saxon potential in r-space, i.e. that has the same elastic scattering S-matrix.

For a real potential, the nuclear phase shifts are related to the algebraic nuclear potential by the following relations:

$$\delta_\ell(k) = \mathrm{Arg}\ \Gamma\ (\ell+1+iv_N(\ell,k)) \qquad (3)$$

$$\delta_\ell(k) = v_N(\ell,k)\psi(\ell+1) + \sum_{n=0}^{\infty} \left[\frac{v_N(\ell,k)}{\ell+1+n} - \mathrm{arctg}\ \frac{v_N(\ell,k)}{\ell+1+n} \right] \qquad (4)$$

where $\delta_\ell(k)$ are the real phase shifts and $\psi(\ell+1)$ is the Digamma-function. For high angular momenta the bracket in the right side of eq. (4) vanishes and we can write

$$\delta_\ell(k) \underset{\ell\to\infty}{\approx} v_N(\ell,k)\psi(\ell+1) \qquad (5)$$

We deduced numerically the algebraic nuclear potential by an iterative method using eq. (4) and (5) that gives exactly the same nuclear phase shifts obtained solving Schrödinger equation for a real Woods-Saxon well.

The real algebraic nuclear potential obtained numerically

in this iterative procedure, can be fitted by the following empirical parametrization:

$$v_N^{real}(\ell,k) = \frac{\exp\left[-\frac{1.6}{\ell_o}\ell\right]\cdot V_R}{1+\left[\frac{\ell_o+1}{\ell+1}\right]\exp\left[\frac{\ell-\ell_o}{\Delta}\right]} \qquad (6)$$

We assumed a similar ℓ-dependence for the imaginary part of $v_N(\ell,k)$.

In figure 1 we present our experimental elastic angular distribution of $^{24}Mg(^{12}C,^{12}C)^{24}Mg$, together with results of AST using the above algebraic potential (eq.2 and 6) (solid line) and of optical model calculations (dashed line). The parameters used in AST approach are $V_R = 2.0$, $V_I = 5.0$, $\ell_o = 14.5$ and $\Delta = 1.7$. The optical potential parameters are V = 10 MeV, $r_o = 1.318$ fm, a = 0.618 fm, W = 23.4 MeV, $r_{oI} = 1.199$ fm and $a_I = 0.552$ fm. Both calculations reproduce well the forward angle region and underestimate the backward cross-section, a feature common to strongly absorbing potentials.

The oscillations and back angle rise could be reproduced by decreasing Δ or V_I, in analogy to sharp edge or surface transparent optical potentials. However our aim was not just reproduce the backward anomaly but get a better understanding of the origin of these anomalies. We will see in the following that the inclusion of α-transfer couplings produces the backward rise in the elastic cross section.

In the case of n coupled reaction-channels, the algebraic potential becomes an nxn symmetric complex matrix. The diagonal elements correspond to potentials producing elastic scattering in channels i = 1,2,...,n and the off-diagonal elements v_{ij} correspond to coupling potentials producing transitions between states i and J. The S-matrix is calculated diagonalizing the matrix $v^{(\ell,\ell)}$. The cross sections $\left[\frac{d\sigma}{d\Omega}\right]_{ij}$ are easily obtained from the elements S_{ij} of the S-matrix.

We used the same ℓ-dependence for the off-diagonal element v_{ij} as in ref. 6. It is a Woods-Saxon derivative ℓ-dependence for the nuclear part and a $\frac{1}{\ell^{\lambda}}$ dependence for the long range Coulomb excitation:

$$v_{ij}(\ell,k) = -\eta^{N}_{ij}\,\frac{d}{d\ell}\left[\frac{U_R+iU_I}{1+\exp\left[\frac{\ell-\ell_o}{\Delta}\right]}\right]_{ij} + \eta^{C}_{ij}\left[\frac{\ell}{\ell_{oC}}\right]^{\lambda+1} \quad \text{for } \ell < \ell_{oC}$$

$$+ \eta^{C}_{ij}\left[\frac{\ell_{oC}}{\ell}\right]^{\lambda} \quad \text{for } \ell > \ell_{oC} \tag{7}$$

where ℓ_{oC} is the Coulomb grazing angular momentum, η^{N}_{ij} and η^{C}_{ij} are the nuclear and Coulomb coupling strengths and λ is the multipolarity of the inelastic excitation. We made some calculation usign Gaussian form factors for the nuclear part of v_{ij} and the conclusions were not affected by the functional form of v_{ij}. Using the rotational frame approximation[7], the spin dependence can be taken into account and the inelastic coupling strengths between states with spins I and J should be proportional to:

$$\eta_{ij} \propto \sqrt{\frac{2\lambda+1}{4\pi}}\;(-1)^{J}\begin{pmatrix} J & \lambda & I \\ 0 & 0 & 0 \end{pmatrix} \langle J\|Q_{\lambda}\|I\rangle \tag{8}$$

The reduced matrix elements $\langle J\|Q_{\lambda}\|I\rangle$ can be related to $B(E\lambda; I\to J)$ for the Coulomb excitation and to β_{λ} for the inelastic nuclear excitation. Then the η_{ij} values can be related to available structure information for the inelastic transitions.

In the following we describe the experimental procedure and results.

We measured at E_{CM} = 25.2 MeV six fairly complete angular

distributions for the system $^{12}C+^{24}Mg$, namely the elastic scattering $^{24}Mg(^{12}C,^{12}C)^{24}Mg_{g.s.}$, the inelastic scatterings $^{24}Mg(^{12}C,^{12}C)^{24}Mg$ (2^+, 1.37 MeV) and $^{24}Mg(^{12}C,^{12}C)^{24}Mg$ (4^++$2'^+$, 4.2 MeV) and the α-transfer reactions $^{24}Mg(^{12}C,^{16}O)^{20}Ne_{g.s.}$, $^{24}Mg(^{12}C,^{16}O)^{20}Ne$ (2^+, 1.63 MeV), $^{24}Mg(^{12}C,^{16}O)^{20}Ne$ (4^+, 4.25 MeV). The beam of ^{12}C was obtained from the São Paulo Pelletron Accelerator and was focussed on an isotopically enriched ^{24}Mg target of 50 $\mu g/cm^2$ evaporated on Carbon backing and containing a small amount of Bi. The outgoing particles were detected by a telescope consisting of a position sensitive ionization chamber followed by Si surface barrier detectors. The backward angle region of the angular distributions was measured detecting the heavier recoil particles ^{20}Ne and ^{24}Mg in the forward hemisphere. The experimental resolution was not sufficient to separate the doublet in ^{24}Mg at 4.12 MeV(4^+) and 4.24 MeV ($2'^+$).

The experimental angular distributions are presented on fig. 2. The elastic and inelastic cross sections present smooth oscillation in the forward angle region and strong rise in intermediate and backward angles. All the transfer reactions have strong rise in the back angle region, presenting angular distributions which are almost symmetrical around 90°.

We performed coupled channels calculations using AST, with 7 channels to reproduce the six measured angular distributions of the $^{12}C+^{24}Mg$ system. The calculated cross sections for the inelastic 4^+ and $2'^+$ states were summed to compare with the experimental angular distribution. In fig. 2 we show the results of these calculations together with the experimental data.

Parameters of the off-diagonal coupling form factors (U_R, U_I, ℓ_o, $\Delta)_{ij}$ (Table 1) were determined by fitting the period, phase and amplitude of oscillations in the forward angle region of inelastic and transfer cross sections. Our experimental data, presenting many well defined oscillations up to the intermediate angle region, allow a very accurate determination of ℓ_o and Δ values of the coupling form factors. We used the same parameters

for all inelastic and transfer transitions respectively, though the ℓ_o of the form factors should decrease with increasing excitation energy. Due to this approximation the oscillations of the 4^+ transfer cross section get out of phase for intermediate angles (see figure 2).

The parameters that define the diagonal matrix elements of the outgoing channel $^{18}O+^{20}Ne$, were determined by fitting the experimental angular distribution[8] of the $^{18}O+^{20}Ne$ elastic scattering at E_{CM} = 22.2 MeV (see fig. 1). The inelastic coupling strengths (Coulomb and nuclear) were calculated from experimental B(Eλ) and β_λ values using eq. (8) and the absolute normalization is obtained by fitting the 2^+ inelastic angular distribution. The hexadecapole deformations (β_4) of ^{24}Mg and ^{20}Ne were also included, producing direct coupling between the 0^+ and 4^+ states. The transfer coupling strengths were adjusted to fit the magnitude of the transfer cross sections. Table II shows the structure informations available and the η_{ij} values used in the seven coupled channels calculation.

The fits are in very good agreement with the data. The absolute magnitude, the period and phase of oscillations and the backward rise are well reproduced. The only cross section which is somewhat under-estimated by the calculations is of the sum of the 4^+ and $2'^+$ states. The coupling strengths were derived from available B(Eλ) and β_λ informations.

In fig. 3 we show the effect on the elastic angular distribution due to the coupling of transfer channels added one by one. We can verify that the backward increase in the elastic cross section comes from the coupling to the transfer states. The contribution of excited transfer states is very important. Similar calculations, coupling only with inelastic 2^+ and 4^+ states, have shown that the effect of the inelastic couplings is much weaker at back angles.

Concluding, we measured six fairly complete angular distributions of elastic, inelastic and α-transfer reactions of the

$^{12}C+^{24}Mg$ system at E_{CM} = 25.2 MeV. We used the AST to couple all the channels measured in our experiment. We determined the form of the nuclear algebraic potential from nuclear phase shifts and its parameters by fitting the incoming and outgoing elastic scattering data. The inelastic coupling strengths were derived from available B(Eλ) and β_λ informations and a good fit was obtained for all channels. The back angle rise in the elastic cross section is fully explained by the coupling between elastic and transfer channels.

References

1. P. Braun-Munzinger and J. Barrette
Phys. Rep. 87, 209 (1982) and references therein.

2. J. Barrette and S. Kahana
Comments Nucl. Part. Phys. 9, 67 (1980) and references therein.

3. R. Lichtenthäler F°, A. Lépine-Szily, A.C.C. Villari and O. Portezan F°
Phys. Rev. C38, 884 (1988).

4. A. Lépine-Szily, R. Lichtenthäler F°, M.M. Obuti, J.M. Oliveira Jr., O. Portezan F°, W. Sciani and A.C.C. Villari
Phys. Rev. C40, 681 (1989).

5. Y. Alhassid, F. Iachello and B. Shao
Phys. Lett. B201, 183 (1988).

6. Y. Alhassid and F. Iachello
Nucl. Phys. A501, 585 (1989).

7. H. Esbensen, S. Landowne and C. Price
Phys. Rev. C36, 1216 (1987).

8. R. Stock, U. Jahnke, D.L. Hendrie, J. Mahoney, C.F. Maguire, W.F. Schneider, D.K. Scott and G. Wolschin
Phys. Rev. C14, 1824 (1976).

9. A. Christy and O. Häusser
Nucl. Data Tables 11, 280 (1973)

10. S.J. Skorka, J. Hertel and T.W. Retz-Schmidt
Nucl. Data 2, 347 (1966);
A.A. Rush and N.K. Ganguly
Nucl. Phys. A117, 101 (1968).

11. Y. Horikawa, Y. Torizuka, A. Mukada, S. Mitsonobu, Y. Kojima and M. Kimura
Phys. Lett. 36B, 9 (1971).

12. P. de Swiniarski, C. Glashausser, D.L. Hendrie, J. Sherman, A.D. Bacher and E.A. McClatchie
Phys. Rev. Lett. 23, 317 (1969).

13. D.K. Olsen, W.R. Phillips and A.R. Barnett
Phys. Lett. 39B, 201 (1972).

14. J. Crossairt, R.D. Bent, A.S. Broad, F.D. Bechetti and J. Jänecke
Nucl. Phys. A261, 373 (1976).

15. J.P. Draayer
Nucl.Phys. A237, 157 (1975).

FIGURE CAPTIONS

Figure 1. Experimental elastic angular distribution of $^{12}C+^{24}Mg$ measured in this work and of $^{16}O+^{20}Ne$ (ref. 8). The solid lines are AST calculations with parameters presented on table I. The dashed line is optical model calculation, its parameters are quoted in text.

Figure 2. Experimental angular distributions of indicated reactions, measured in this work. The solid lines are the result of the calculations coupling seven reactions channels in the AST scheme. Parameters used are presented on tables I and II.

Figure 3. Experimental elastic angular distribution of $^{12}C+^{24}Mg$. The dashed-dot line is the result of AST calculation without any couplings, the dotted line with coupling between elastic and ground-state transfer channels, dashed line with couplings to 0^+ and 2^+ transfer states, solid line with couplings to 0^+, 2^+ and 4^+ transfer states.

TABLE CAPTIONS

Table I. The reactions channels with parameters characterizing the diagonal elements v_{jj} and off diagonal elements v_{ij}.

Table II. The available structure informations and the coupling strenghts used in the AST calculations. They were deduced using equation 8 and normalized for the first $0^+ \rightarrow 2^+$ inelastic transition. Couplings not quoted were not considered in the calculation.

Table I

Channel n° J	Reaction Channel I → J	Q	Diagonal Elements v_{IJ}					Off-diagonal elements v_{IJ}			
			V_R	V_I	ℓ_o	ℓ_{oc}	Δ	U_R	U_I	ℓ_o	Δ
1	$^{12}C+^{24}Mg \rightarrow ^{12}C+^{24}Mg(0^+)$	0	2.0	6.0	14.5	10.0	1.7	6.0	1.5	17.5	0.9
2	$^{12}C+^{24}Mg \rightarrow ^{12}C+^{24}Mg(2^+)$	-1.37	2.0	6.0	14.5	10.0	1.7	6.0	1.5	17.5	0.9
3	$^{12}C+^{24}Mg \rightarrow ^{12}C+^{24}Mg(4^+)$	-4.12	2.0	6.0	14.5	10.0	1.7	6.0	1.5	17.5	0.9
4	$^{12}C+^{24}Mg \rightarrow ^{12}C+^{24}Mg(2'^+)$	-4.24	2.0	6.0	14.5	10.0	1.7	6.0	1.5	17.5	0.9
5	$^{12}C+^{24}Mg \rightarrow ^{16}O+^{20}Ne(0^+)$	-2.15	2.0	6.0	14.0	10.0	1.5	8.0	1.5	18.85	0.4
6	$^{12}C+^{24}Mg \rightarrow ^{16}O+^{20}Ne(2^+)$	-3.78	2.0	6.0	14.0	10.0	1.5	8.0	1.5	18.85	0.4
7	$^{12}C+^{24}Mg \rightarrow ^{16}O+^{20}Ne(2^+)$	-6.40	2.0	6.0	14.0	10.0	1.5	8.0	1.5	18.85	0.4

Table II

Nucleus	Inelastic Transitions i → j	B(Eλ; i→j) $e^2 fm^{2\lambda}$	β_λ	η^C_{ij}	η^N_{ij}
^{24}Mg	$0^+ \to 2^+$ (1.37 MeV)	430[a]	+0.45[c,d]	-0.27	0.081
	2^+ (1.37 MeV) $\to 4^+$ (4.12 MeV)	106[b]		-0.60	0.18
	$0^+ \to 4^+$ (4.12 MeV)	1100[c]	-0.05[c,d]	+0.24	-0.01
	$0^+ \to 2^+$ (4.24 MeV)	25[b]		-0.065	0.02
^{20}Ne	$0^+ \to 2^+$ (1.63 MeV)	370[e]	+0.40[c,d]	-0.25	0.074
	2^+ (1.63 MeV) $\to 4^+$ (4.25 MeV)	94[b]		-0.55	0.164
	$0^+ \to 4^+$ (4.25 MeV)	10990[c]	+0.19[c,d]	-0.74	0.044

Transfer Transitions i → j	$S_q(^{24}Mg(i) = {}^{20}Ne(j)+\alpha)$		η^C_{ij}	η^N_{ij}
	S_q(exp)	S_q(theor)		
$^{24}Mg(0^+) \to {}^{20}Ne(0^+)$	0.21[f]	0.35[g]	0	0.0275
$^{24}Mg(0^+) \to {}^{20}Ne(2^+)$	0.19[f]	0.05[g]	0	0.046
$^{24}Mg(0^+) \to {}^{20}Ne(4^+)$	0.87[f]	0.28[g]	0	0.068
$^{24}Mg(2^+) \to {}^{20}Ne(0^+)$	-	0.13[g]	0	0.018
$^{24}Mg(4^+) \to {}^{20}Ne(0^+)$	-	0[g]	0	0

a - Ref. 9 b - Ref. 10 c - Ref. 11
d - Ref. 12 e - Ref. 13 f - Ref. 14
g - Ref. 15

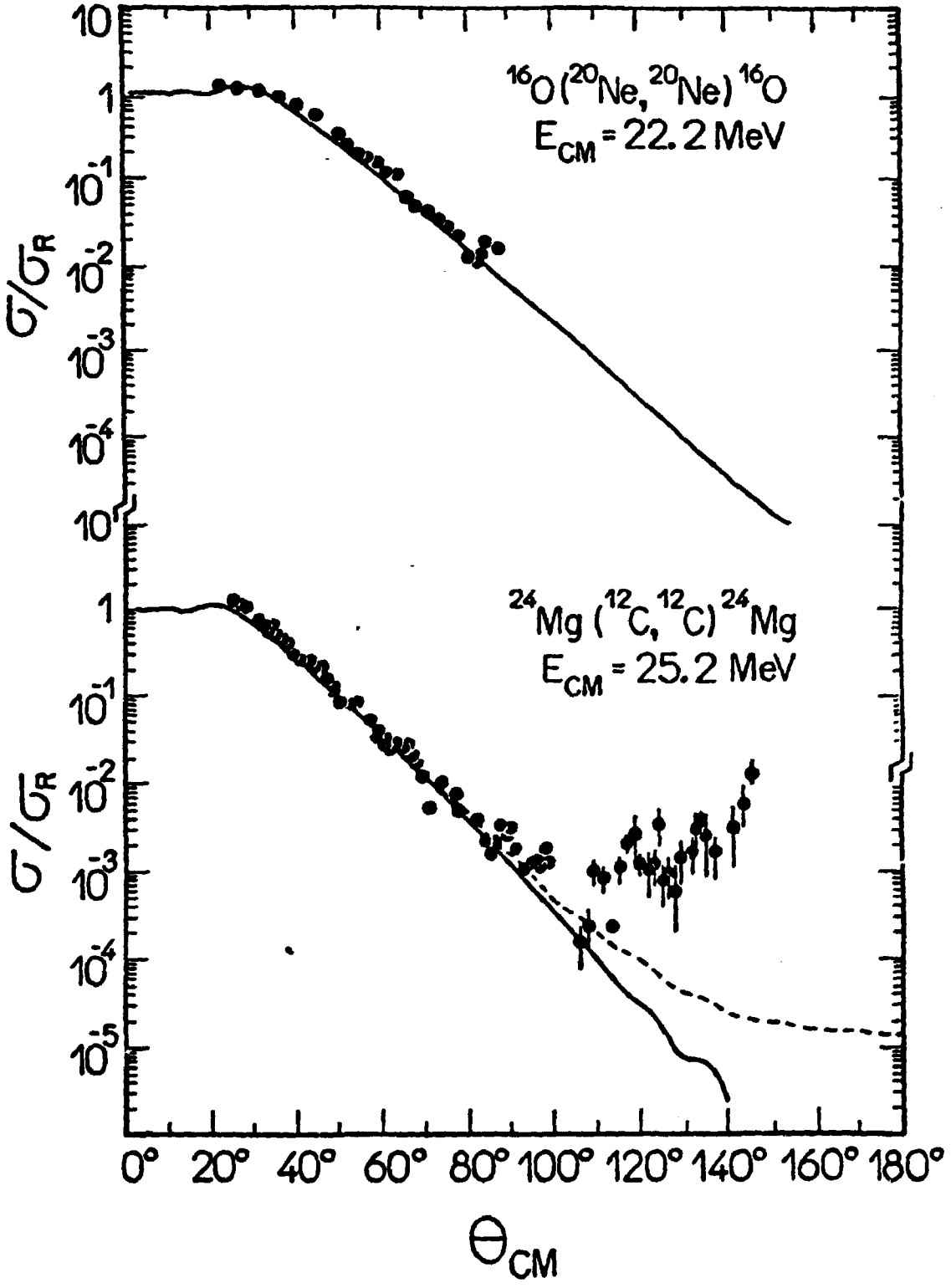
$^{16}O(^{20}Ne,^{20}Ne)^{16}O$
$E_{CM} = 22.2$ MeV
$^{24}Mg(^{12}C,^{12}C)^{24}Mg$
$E_{CM} = 25.2$ MeV
σ/σ_R
σ/σ_R
10
1
10^{-1}
10^{-2}
10^{-3}
10^{-4}
10^{-5}
0° 20° 40° 60° 80° 100° 120° 140° 160° 180°
Θ_{CM}

Fig 1

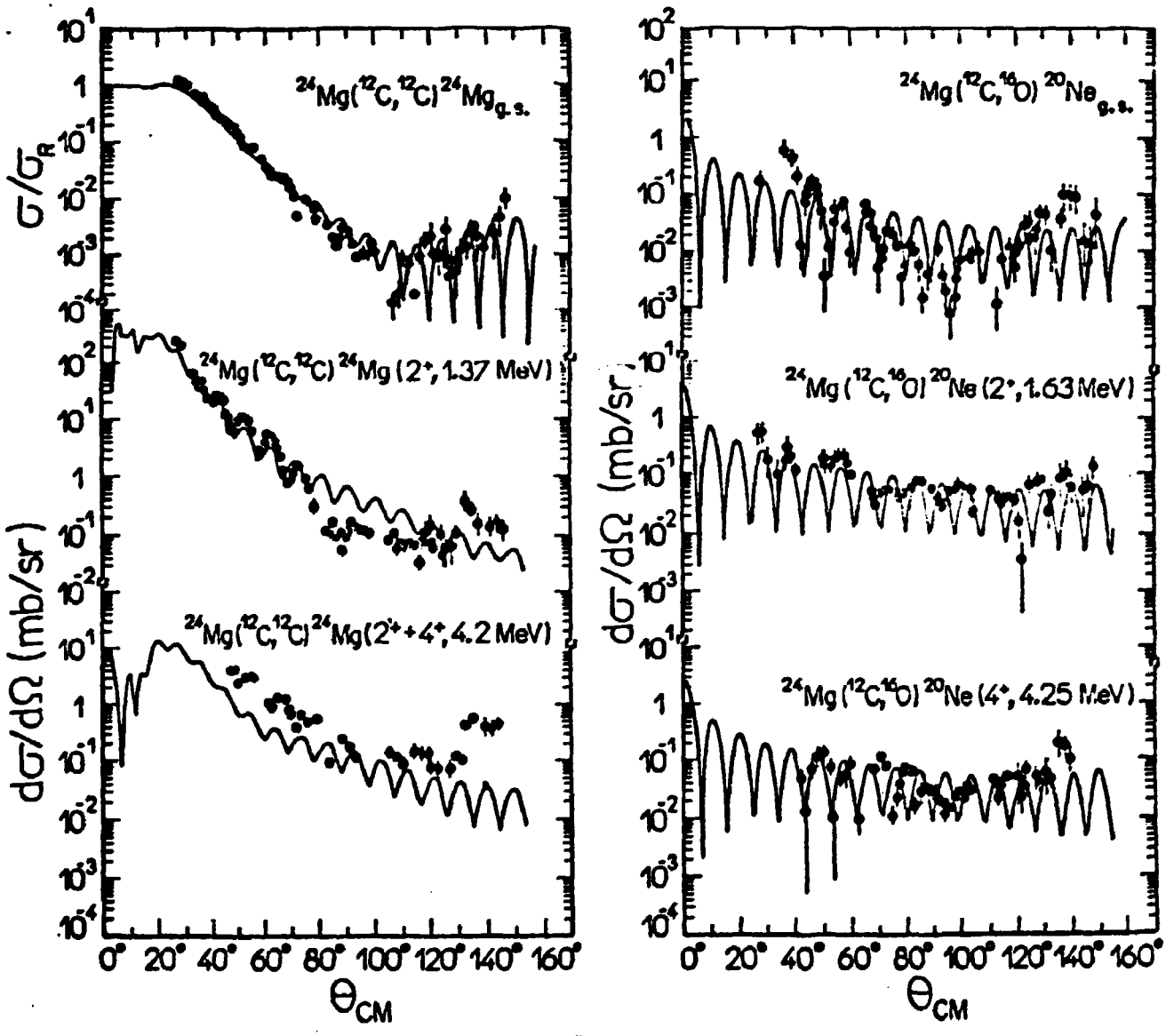
$^{24}Mg(^{12}C,^{12}C)^{24}Mg_{g.s.}$
$^{24}Mg(^{12}C,^{12}C)^{24}Mg(2^+,1.37\ MeV)$
$^{24}Mg(^{12}C,^{12}C)^{24}Mg(2^+ + 4^+,4.2\ MeV)$
σ/σ_R
$d\sigma/d\Omega$ (mb/sr)
Θ_{CM}
$^{24}Mg(^{12}C,^{16}O)^{20}Ne_{g.s.}$
$^{24}Mg(^{12}C,^{16}O)^{20}Ne(2^+,1.63\ MeV)$
$^{24}Mg(^{12}C,^{16}O)^{20}Ne(4^+,4.25\ MeV)$
$d\sigma/d\Omega$ (mb/sr)
Θ_{CM}

Fig 2

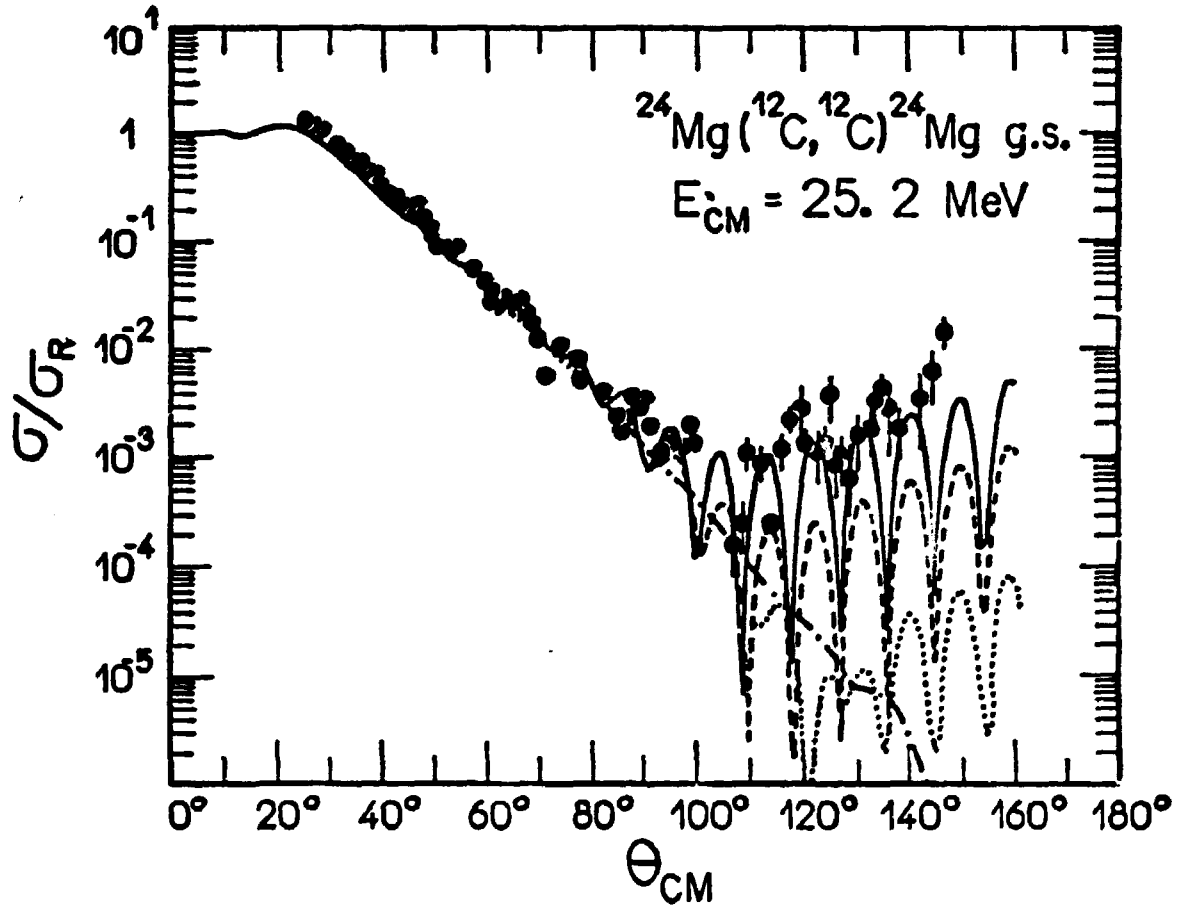
$^{24}Mg(^{12}C,^{12}C)^{24}Mg$ g.s.
E_{CM} = 25.2 MeV
σ/σ_R
10^{1}
1
10^{-1}
10^{-2}
10^{-3}
10^{-4}
10^{-5}
0° 20° 40° 60° 80° 100° 120° 140° 160° 180°
θ_{CM}

Fig. 3